Stepwise Dissociation of Thermally Activated Phenol on Pt(111)

H. Ihm and J. M. White*

Center for Materials Chemistry, Department of Chemistry and Biochemistry, University of Texas at Austin, Austin, Texas 78712

Received: February 10, 2000

The thermal reactions of phenol on Pt(111), including reaction intermediates, have been studied between 125 and 1100 K by using phenol-h_6, phenol-*2,4,6*-d_3, phenol-*2,3,4,5,6*-d_5, and phenol-d_6 with temperature-programmed desorption (TPD), high-resolution electron energy loss spectroscopy (HREELS), and X-ray photoelectron spectroscopy (XPS). Phenol adsorbs molecularly at 125 K, with the ring plane parallel to the surface. During heating, the O−H bond breaks below 200 K. The O−H bond dissociation product, phenoxy, has a quinoidal structure with η^5-π-adsorption geometry via the C2 through C6 atoms with the C1 atom tilted away from the ring plane. Bonds in the phenoxy species rearrange toward oxocyclohexadienyl upon heating. The reactivity of phenoxy depends on the initial phenol coverage. Below 0.5 monolayer (ML), phenoxy fully decomposes to CO(g), H_2(g), and C(a). Above 0.7 ML coverages, it follows two different pathways: (1) 85 ± 7% forms CO(g), H_2(g), C_2(a), and C_3H_3(a) at 490 K, the latter dehydrogenating to H_2(g) and C(a) above 550 K, and (2) 15 ± 7% forms C_6H_6(g) and O(a) between 380 and 530 K. TPD and HREELS of isotopically labeled phenol indicate selective C2−H and C3−H dissociation within phenoxy. The common vibrational spectra and desorption features above 550 K during TPD of phenol, iodobenzene, and benzene strongly suggest a common intermediate species, C_3H_3. After annealing to 1100 K, only carbidic C remains.

Introduction

Phenol surface chemistry is interesting because when its reactions are catalyzed by metals, there can be a number of different initial bond-breaking processes, e.g., O−H, C−O, C−H, and C−C. From the initial step, several reaction paths may ensue leading to a variety of products, some of which desorb. The competition among the paths depends on the initial coverage of phenol.

There have been studies of phenol on metal and semiconductor surfaces.[1−16] Two of these involve Pt(111).[1,2] The high-resolution electron energy loss spectroscopy (HREELS) study by Zhuang[1] showed no O−H stretching mode at 255 K indicating complete O−H bond scission at or below that temperature. Lu et al.[2] used Auger spectroscopy, low-energy electron diffraction (LEED), and HREELS to examine phenol adsorbed on a Pt(111) electrode from millimolar solutions at room temperature. They observed an ordered structure, (3×3) LEED pattern. From the LEED and HREELS data, they found that the saturation packing was 0.12 phenol per surface Pt atom with the phenol ring lying flat on the surface.

Many studies have focused on the adsorption geometry of phenol or phenoxy. On most surfaces, e.g., Ni(111),[13] Cu(110),[14] and Pt(111),[1] ensemble averages place the ring of phenol or phenoxy nearly parallel to the surface plane. Mo(110)[9] and Ag(110) at 225 K[15] are exceptions; on Mo(110) the phenoxy ring is tilted 60° from the surface plane at 100 K and on Ag(110), upon annealing phenol to 225 K, the ring tilted at 40°. Locally, geometries may differ. For example, an STM study on Cu(110)[5] reveals regions where the local coverage is between 0.25 and 0.33 phenoxy per surface Cu atom with different ring orientations (from nearly parallel to almost normal) to the surface plane.

Typically, the first reaction of adsorbed phenol is O−H bond dissociation analogous to adsorbed alcohols. The reactivity of the resulting phenoxy species depends on the surface. On Mo(110),[8] the only overall reaction products are desorbed H_2 and surface carbon and oxygen. On Rh(111)[3] and Ni(110),[7] phenoxy reacts to desorb CO and H_2, leaving surface carbon. On Al(111),[11] H_2 and C_6H_6 desorb while C and O remain adsorbed. On Ni(111),[13] the desorbing products are H_2, CO, and unknown hydrocarbons. In only a few cases have detailed mechanisms, the goal of the present work, been established.[7,11,12] On Al(111), phenoxy decomposition was initiated by the dissociation of the C−O bond followed by one ortho-position C−H bond dissociation. On Ni(110), phenoxy decomposition was initiated by breaking an ortho- or para-C−H bond.

From this review, phenol generally adsorbs with the ring parallel to the metal surface, and during heating the O−H bond breaks first, leaving adsorbed phenoxy. On a surface with a very strong O−metal bond, e.g., Mo(110), the phenoxy species is bonded to the surface via O, the ring tilts away from the surface plane, and the C−O bond dissociates, leaving surface oxygen. When the O−metal bond is weaker and the surface can easily accommodate CO and hydrogen, e.g., Rh(111) and Ni(110), the products are H_2(g), CO(g), and surface carbon. However, the number, intensity, and temperature of H_2 desorption peaks differ for various surfaces implying different reaction pathways. For example, ordered according to increasing peak temperature, the peak area ratios are 1:1:4 on Al(111), 1:3:1:1 on Ni(110), 2:1:3 on Mo(110), and 1:3:1:1 on Rh(111). In most cases, C−C bonds begin to break after at least one C−H bond breaks.

Isotopic labeling of H in phenol can be used to probe the ortho-, meta-, and para-selectivity of C−H bond breaking during temperature-programmed desorption of molecularly adsorbed phenol. In this paper, we show, using deuteration at various positions, that the reactivity of phenoxy on Pt(111) differs from other surfaces in that a unique combination of desorption products—H_2, CO, and C_6H_6—are observed. Unlike on Al(111)

10.1021/jp0005423 CCC: $19.00
Published on Web 06/10/2000

SCHEME 1: Isotopically Labeled Forms of Phenol

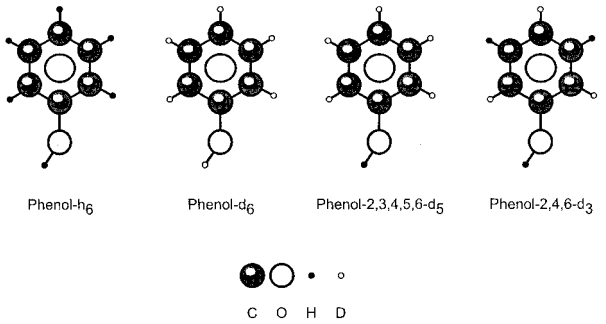

and Ni(110), the first C−H bonds that break are at the C2 and C3 positions in phenoxy. In this paper, we discuss the unique reactivity and geometry of phenoxy species on Pt(111).

Experimental Section

The experiments were carried out in an ultrahigh vacuum chamber with a base pressure of 3×10^{-10} Torr. The system was equipped with temperature-programmed desorption (TPD), high-resolution electron energy loss spectroscopy (HREELS), X-ray photoelectron spectroscopy (XPS), and low-energy electron diffraction (LEED) capabilities. Further details are available elsewhere.[17]

The Pt(111) crystal was 8 mm in diameter and 1.5 mm thick. The sample was cleaned twice by sputtering with 3 keV Ar^+ at 500 K for 5 min and annealing at 1150 K for 5 min. Then the sample was examined with LEED, XPS, and HREELS to assess surface crystal order and surface cleanliness.

The crystal temperature was monitored by a chromel−alumel thermocouple spot-welded to the back of the crystal. Using thermal contact to liquid nitrogen, the base temperature was between 110 and 120 K. The sample was heated resistively, and the TPD ramp rate was 3 K s^{-1}. HREELS measurements were taken with a primary beam energy of 3 eV and a typical resolution of 100 cm^{-1} full width at half-maximum (fwhm). XPS data were taken with Al Kα photons (1486.6 eV) and a hemispherical analyzer with a step size of 0.01 eV. For C1s and Pt4f measurements, 50 eV pass energy was applied, while for O1s, 80 eV was applied to enhance a relatively weak signal. All binding energies are referenced to a $Pt4f_{7/2}$ binding energy of 70.9 eV.[18]

Phenol (99+%, EM science), phenol-d_6 (99+ atom % D, Aldrich), phenol-*2,3,4,5,6*-d_5 (98 atom % D, Aldrich), and phenol-*2,4,6*-d_3 (98 atom % D, Aldrich) were used after several freeze−pump−thaw purifications. (See Scheme 1) Note that the H/D in hydroxy group is exchangeable. In fact, phenol-d_6 contained some phenol-d_5 and showed H incorporation in TPD. Phenol isotopes were dosed through a 10 (± 2) μm pinhole positioned about 1 cm from the sample surface. The pressure behind the pinhole was kept at 0.4 Torr, monitored by a thermocouple gauge in the dosing line.

Absolute surface coverages of phenol (phenol per surface Pt (Pt_s) or phenol cm^{-2}) were determined from C1s XPS peak areas and a calibration using a reference Pt(111) surface saturated with CO at 300 K, for which the absolute coverage is 0.49 ± 0.02 (one CO molecule per two surface platinum atoms).[19] In this study, 1 ML (monolayer) is defined as a single layer of phenol on the surface and corresponds to the coverage just before molecular desorption in TPD. Similarly 2 ML corresponds to the saturation coverage of a 225 K desorption peak (see below). Above 2 ML, there is an unsaturable peak growing at about 190 K. The desorbed amount increases linearly with dose above 1 ML coverage. The C1s XPS area also grows linearly with dose. Both indicate that the sticking coefficient of phenol is constant. One monolayer corresponds to 0.96 carbon atoms per surface platinum atom (0.16 phenol-d_6/Pt_s). This absolute ML coverage was assumed to be the same for all the labeled phenols.

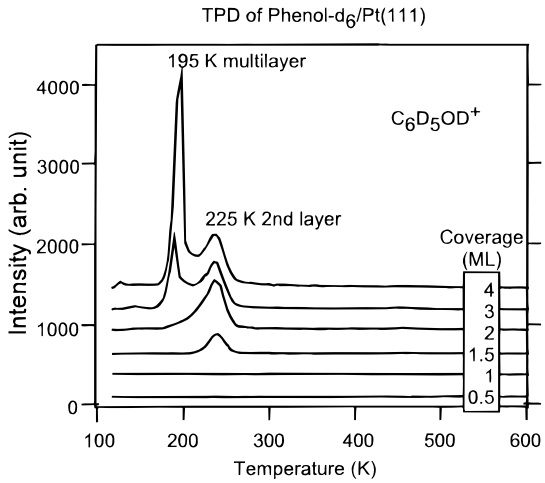

Figure 1. Molecular desorption, $m/z = 100$, of phenol-d_6 dosed on Pt(111) at 110 K. The coverage increases from bottom to top: 0.5, 1, 1.5, 2, 3, and 4 ML. The absence of desorption between 300 and 500 K shows total dissociation of the first layer upon heating. The second layer desorption peak is at 225 K, independent of coverage, and the multilayer desorption peak is about 30 K lower and slowly moves upward as the coverage increases.

The absolute amounts of other desorption species were determined by TPD. As a reference, the saturation coverage of CO (0.49 CO/Pt_s at 300 K)[19] is already known. The saturation coverage of benzene is 0.16 per Pt_s: 45% of the monolayer desorbs molecularly and 55% of the monolayer dehydrogenates, producing H_2 upon heating.[20] The desorption peak areas of CO, C_6D_6, and D_2 from phenol doses were measured and compared with the reference peak areas.

Results

Figure 1 shows the TPD of $m/z = 100$ ($C_6D_5OD^+$) from phenol-d_6 as a function of coverage. Using our definition, there is no molecular desorption up to 1 ML. There is a saturable desorption peak at 225 K, which we ascribe to the second layer. Finally, there is an unsaturable peak at 183 K that shifts to higher temperatures with increasing dose. This is assigned to multilayer desorption. Using Redhead analysis,[21] the calculated desorption energies (E_d) for the second and multilayer peaks were 57.3 and 49.4 kJ mol^{-1}, respectively. The desorption energy for multilayers is, as expected, slightly higher than the enthalpy of vaporization of liquid phenol (45.69 kJ mol^{-1}).[22]

On the basis of calibrated XPS data, Figure 2 and the inserted table show the absolute (C/Pt_s) ratio for 1 and 4 ML of phenol-d_6 as a function of flashing temperature. For 1 ML initial coverage, the ratio does not drop until 400 K, consistent with the absence of desorption of C-containing species. The slight rise between 125 and 180 K is attributed to the small amounts of background CO adsorption. The decay above 400 K is consistent with the desorption of C-containing species (see below). Turning to the 4 ML coverage, the initial ratio of 3.75 decreases to 2.09 after flashing to 200 K, consistent with multilayer desorption at 195 K. Upon desorption of the second layer by heating to 300 K, the ratio further decreases to 1.15. Between 400 and 1100 K, the 4 and 1 ML curves coincide. On

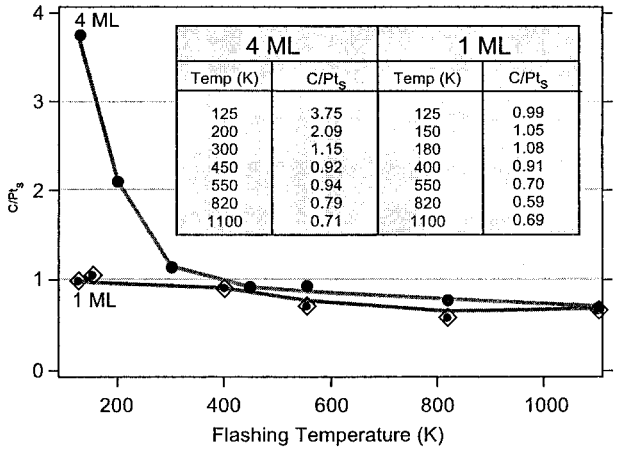

4 ML		1 ML	
Temp (K)	C/Pt$_s$	Temp (K)	C/Pt$_s$
125	3.75	125	0.99
200	2.09	150	1.05
300	1.15	180	1.08
450	0.92	400	0.91
550	0.94	550	0.70
820	0.79	820	0.59
1100	0.71	1100	0.69

Figure 2. For phenol-d_6 on Pt(111), the ratio, C/Pt$_s$ (Pt$_s$ denotes a surface Pt atom), after flashing to temperatures. The lines are guides to the eye. The average absolute coverage of 1 ML, calibrated by saturated CO/Pt XPS, is 0.16 phenol-d_6/Pt$_s$, which is 0.96 C/Pt$_s$. The 0.7 C/Pt$_s$ ratio at 1100 K shows that 73% of the carbon in the first layer of phenol remains after flashing to 1100 K.

an absolute scale, the average (C/Pt$_s$) ratio for 1 ML of phenol-d_6 is 0.96 (0.16 phenol-d_6/Pt$_s$). While previous study of phenol adsorbed on a Pt(111) electrode from millimolar solution reported 0.12 phenol/Pt$_s$ as the saturation packing,[2] the saturation coverage was 0.16 for benzene on Pt(111)[20] and phenol on Ni(110).[7] At 1100 K, C/Pt$_s$ is 0.70, corresponding to 73% of the C in 1 ML of phenol.

Besides phenol, the other desorption products were dihydrogen, carbon monoxide, and benzene (Figure 3). The only other desorption was a tiny amount of water that appeared between 165 and 190 K and is attributed to source contamination since dosed water desorbs in this region.[23]

Figure 3A shows the desorption of isotopic dihydrogen species for submonolayer to multilayer doses of phenol-d_6. The H_2 signal peaking between 250 and 350 K is ascribed to background hydrogen. Dideuterium desorption shows four easily recognizable peaks, <350, 490, 540, and 620 K. The peak below 350 K is assigned to the recombination of deuterium atoms[24] that become attached to Pt when O−D bonds break at lower temperatures. There is corresponding, and more intense, HD desorption below 350 K. The H is attributed to a combination of background hydrogen adsorption during dose and H for D isotope exchange in the hydroxy group of phenol. The low-temperature HD and D_2 peaks shift downward with increasing dose up to 2 ML. This is attributed to two effects: second-order hydrogen atom recombination kinetics and destabilization of H−Pt bonds due to local crowding.

The three other peaks at 490, 540, and 620 K are from the deuterium in the phenyl ring. The 490 K peak contains ~4% H that is attributed to exchange of H from background for D in the phenyl ring. This exchange is ignored hereafter. The 540 and 620 K peaks contain negligible H. For phenol-h_6, the peak corresponding to the 490 K peak from phenol-d_6 is lower by 5 K (not shown) indicating a small kinetic isotope effect. Compared to the low-temperature hydrogen desorption, the 490 K peak shifts in the opposite direction with coverage, from 470 K (0.5 ML) to 490 K (1 ML), and remains constant above 1 ML. Since this desorption is reaction-limited, the peak shift is ascribed to an effective activation energy increase with coverage. Finally, the peak at 620 K is very broad, extending to 820 K.

Figure 3B shows CO TPD data for four coverages. There are two peaks and a high-temperature shoulder. The lowest peak at 420 K corresponds to CO desorption from Pt. The major peak

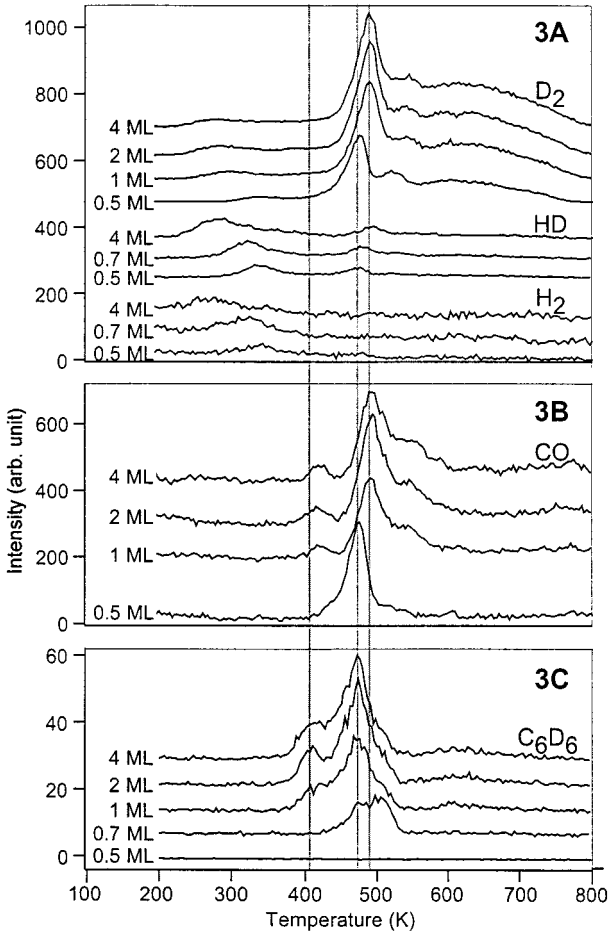

Figure 3. Desorption products from phenol-d_6 dosed on Pt(111) at 120 K and various coverages: (A) H_2, HD, and D_2, (B) CO, and (C) benzene-d_6.

correlates with the 490 K D_2 desorption including the shift from 470 K (at 0.5 ML) to 490 K at 1 ML. Above 1 ML, the peak position remains constant and the intensity saturates at 2 ML. Above 1 ML, a shoulder emerges peaking at 550 K. This 550 K peak is nearly coincident with the small D_2 peak at 540 K. The 420 K peak cannot be assigned solely to background CO adsorption. Much of this peak, and the entirety of the higher temperature CO, is due to C−C bond cleavage in phenol.

Figure 3C shows benzene-d_6 desorption as a function of coverage. Benzene desorption first appears at 0.7 ML as a broad desorption with a maximum near 500 K. At 1 ML, much more benzene desorbs and the distribution shifts to lower temperatures with peaks at 400 and 470 K. As mentioned in the Experimental Section, D replacement by H in OH contributes to isotopic $C_6H_{6-x}D_x$ desorption (not shown). The 400 K benzene peak contains much more H than the 470 K benzene peak (not shown). As discussed below, the local coverage and the rate of C−H bond breaking control the distribution of the benzene desorption. Benzene desorption approaches saturation above 2 ML.

The TPD areas of each desorption product as a function of coverage are shown in Figure 4. Molecular desorption varies linearly with coverage above 1 ML (dashed line). To account for H-for-D exchange, we summed the $m/z = 4$ and $m/z = 3$ amu signals to compute the total amount of dihydrogen desorbed (closed circles). Comparing the TPD area of each desorption product at 2 ML (saturation) with reference TPD area data (as explained in the Experimental Section), the calculated desorption amounts are 0.40 D_2, 0.12 CO, and 0.0098 C_6D_6 per Pt$_s$ atom.

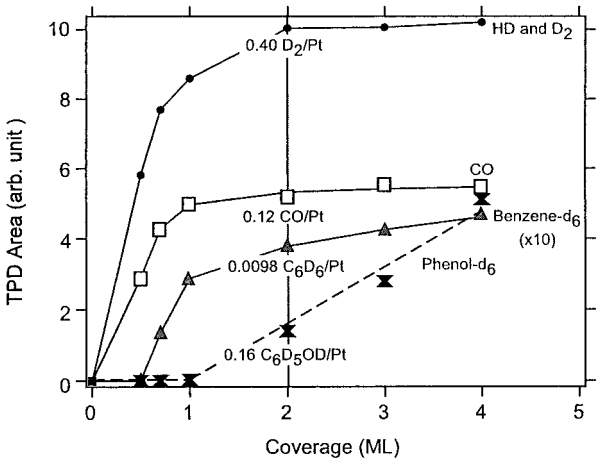

Figure 4. TPD area of desorption species from phenol-d_6 dosed on Pt(111) as a function of initial coverage. Molecular hydrogen species and CO desorption occurs even at low coverages, while benzene desorption starts above 0.5 ML and phenol desorption starts above 1 ML. Phenol desorption varies linearly with the dose above 1 ML (shown as dashed line). The absolute desorption amounts, in terms of molecules per Pt_s, for an initial phenol coverage of 2 ML are indicated along the vertical line.

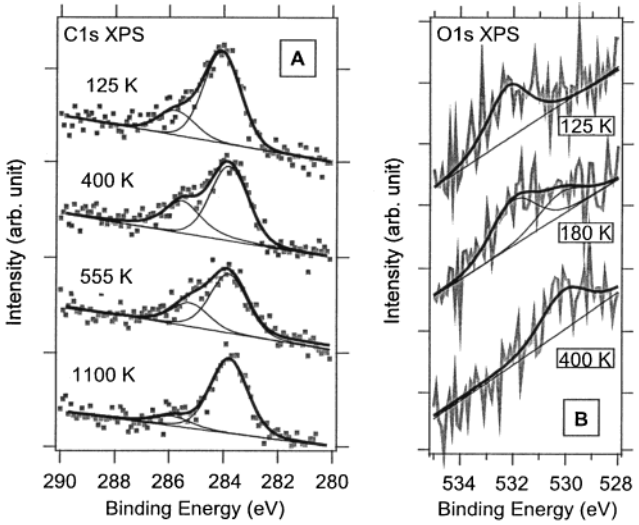

Figure 5. C1s (A, gray dots) and O1s (B, gray lines) XPS annealing set of 1 ML phenol-d_6 on Pt(111). C1s spectra are fit with peaks with 1.6 eV fwhm, and O1s spectra are with 2.0 eV fwhm (thin black lines). The sum (thick black lines) of each fit components are compared with raw data (gray).

H-labeled benzene up to at least $C_6H_4D_2$ appeared in the 400 K peak and up to $C_6H_2D_4$ in the 470 K peak with the relative ratio of 100/40/28/6/0.25 corresponding to $C_6D_6/C_6HD_5/C_6H_2D_4/C_6H_3D_3/C_6H_4D_2$ (not shown). Including all the isotopic forms, the total benzene desorption is 0.017 benzene per Pt_s. The total is nearly a factor of 2 larger than C_6D_6 and is taken as reflecting the significance of H made available through O−H dissociation, the O−H formed by H-for-D exchange before and during dosing. The total H incorporation in benzene desorption is 3.5% of the D available in the initial phenol. Therefore, H-for-D exchange in the phenyl ring can be ignored in discussing the C−H/C−D bond dissociation selectivity on the basis of phenol-*2,4,6*-d_3 data.

Elemental analysis, undertaken for a 2 ML dose after subtracting the contribution of the second layer, gave the following percentages of the total available from 1 ML phenol (0.16 phenol/Pt_s) that desorbs: 93% D (D_2 and benzene), 23% C (CO and benzene), and 75% O (CO). Since, by XPS, 73% of the C remains adsorbed after annealing to 1100 K, the total amount of C detected by summing XPS and TPD is 96%. Thus, within experimental uncertainties, the total amounts of D and C are accounted for. Owing to low XPS sensitivity, we could not determine residual O, but the TPD elemental analysis supports the idea that approximately 25% of the C−O bonds dissociate upon heating, leaving some adsorbed O. Interestingly, while there is no molecular desorption of monolayer phenol, typical aliphatic alcohols—methanol, ethanol, propanol, and *n*-butanol—all show parent desorption for monolayer coverage on Pt(111).[25,26]

Figure 5A shows C1s XPS of 1 ML phenol-d_6/Pt(111) as a function of flashing temperature. Up to 180 K (not shown), the spectra can be fit with two peaks (285.8 and 284.1 eV) with an area ratio of 1:5. We assigned the 285.8 eV peak to the C bonded to O and the 284.1 eV peak to other carbons in the ring. Our observations agree with other studies that observed 284.4 and 285.9 eV peaks on Ag(110)[15] and 290.4 and 292.0 eV peaks in the gas phase.[27] The spectrum after flashing the 4 ML phenol to 300 K has the same peak intensities and positions (not shown). After flashing to 400 K, the C1s peaks shift to lower binding energies by 0.3 eV, implying a change in the adsorption states. The peak at 285.5 eV shifts further to 285.1 eV after flashing to 550 K. Compared to the initial intensity, the C1s signal decreases by 8% at 400 K and by 29% at 550 K, consistent with some benzene desorption before 400 K and large CO and benzene desorption at 490 K. After flashing to 1100 K, there is only one peak at 283.8 eV (graphitic carbon)[28] with 73% of initial C intensity. The peak at 286 eV after 1100 K anneal (and cooling) is ascribed to background CO adsorption during XPS.

Figure 5B shows O1s XPS raw data and fitted curves with 2 eV full width at half-maximum. As for adsorbed H_2O,[23] 532.2 eV at 125 K is consistent with molecular phenol. After flashing to 180 K, the peak broadens and can be fit with two curves at 532.0 and 530.2 eV. For phenol on Rh(111), two different chemical states of O were found after annealing to 250 K.[3] The two peaks are assigned to molecularly adsorbed phenol and phenoxy arising from O−H bond cleavage. Interestingly, the peak shift is opposite that for methoxy formation on Pt(111) where the O1s peak shifts from 532 to 533 eV as methanol forms methoxy.[25] This difference suggests very different O atom environments for phenoxy and methoxy. After flashing to 400 K, the O1s spectrum can be fit with a single peak (530.1 eV) consistent with one chemical species, phenoxy. Insignificant changes in the position compared to the peak at 180 K (530.2 eV) imply minimal change in O chemical state. After flashing to 500 K, the signal decreases drastically (cannot be detected above the noise). This is consistent with major CO desorption (75% of 1 ML phenol) below 500 K.

The O−H bond in phenol on Pt(111) was reported to be completely dissociated at 255 K.[1] To determine whether the dissociation occurs upon adsorption or is thermally activated, we took HREELS of 0.5 ML phenol after dosing at 125 K and after flashing to 200 K (Figure 6). The O−H mode at 3300 cm^{-1} is strong at 125 K but absent at 200 K, confirming that dissociation occurs between 125 and 200 K. The assignment of other modes is postponed until Figure 10 below.

Figure 7 shows TPD of (HD + D_2) from 2 and 0.5 ML phenol-d_6 on Pt(111). For reasons noted earlier, we summed the TPD signals of $m/z = 3$ and 4 to calculate the total dihydrogen desorption. While the TPD signals exhibit four local maxima, only three components were used because the peak at 550 K was always very small (<0.5 D) and uncertain. Since

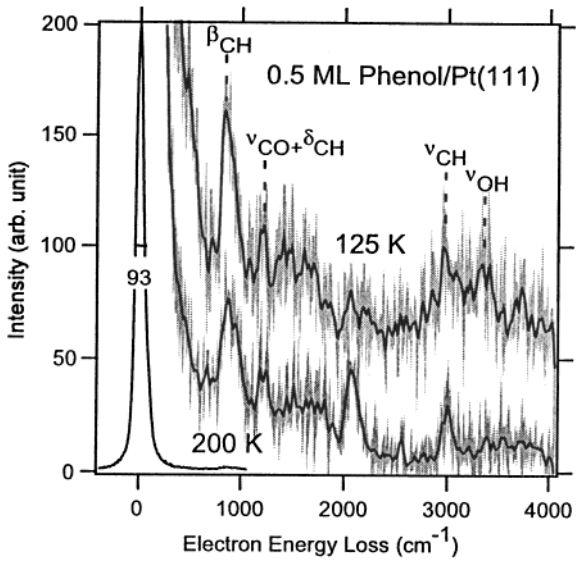

Figure 6. HREELS of 0.5 ML phenol on Pt(111) at 125 K and after flashing to 200 K. The disappearance of the OH stretching mode at 3300 cm^{-1} after flashing confirms O−H bond scission below 200 K. Raw data (gray) are smoothed (black) to reduce noise.

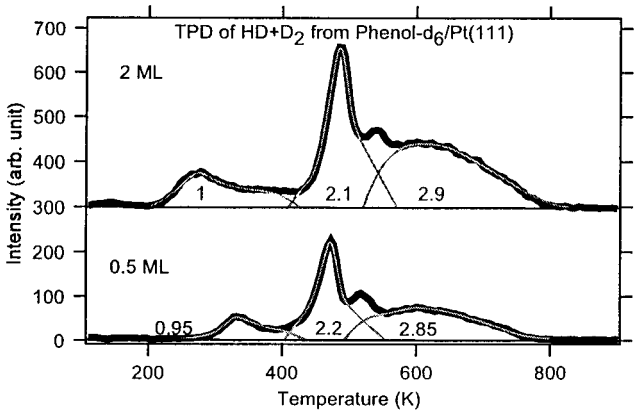

Figure 7. Deuterium desorption peaks from 0.5 and 2 ML of phenol-d_6 on Pt(111), shown in thick black lines. To get the effective total contribution of D, we summed the HD and D_2 signals. The total peak area of 2 ML is twice of that of 0.5 ML. The desorption peak can be decomposed into three peaks at 300, 450, and 620 K with close to 1:2:3 relative area ratio (thin gray lines). The ratio suggests a stoichiometric stepwise dehydrogenation process for each phenoxy.

the benzene-d_6 desorption is much smaller than the D_2 desorption, we did not take into account D forming benzene-d_6. Both sets of data give 1:2:3 ratio of peaks at 300, 490, and 620 K, respectively. As constructed, the peak at 550 K in the raw data contains contributions from both the 490 and 620 K components. The first peak (300 K) is assigned to D in the hydroxyl group. The two remaining peak fits, one broad and one narrow, suggest that phenoxy undergoes stepwise dehydrogenation. Assuming each phenoxy acts independently, there are four possible initial phenoxy dehydrogenation pathways that lead to an *average* loss of two D's from each phenoxy as required by the 490 K desorption intensity:

(1) two ortho-position C−D bonds dissociate

(2) two meta-position C−D bonds dissociate

(3) neighboring ortho- and meta-position C−D bonds dissociate

(4) neighboring meta- and para-position C−D bonds dissociate

By using TPD and HREELS, we eliminated paths 1 and 2

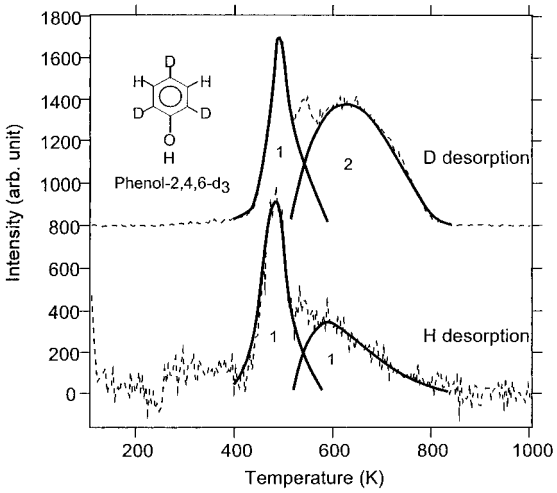

Figure 8. TPD (dotted lines) of H and D from phenol-*2,4,6*-d_3 on Pt(111) where H = 2(signal of 2 amu) + (signal of 3 amu) and D = 2(signal of 4 amu) + (signal of 3 amu). To remove contributions from background H and OH in phenol, the 2 and 3 amu signals from phenol-d_5 were subtracted. The thick black lines are fits.

(see below). Later in the discussion section, we will show that path 3 is favored.

To assess which, if any, of these four paths dominates the dehydrogenation, we used partially deuterated phenol. The phenol-*2,3,4,5,6*-d_5 TPD spectrum (not shown) shows clear H_2 desorption at 300 K (desorption limited) with HD and D_2 desorption at higher temperatures. The plot in Figure 8 shows calculations based on phenol-*2,4,6*-d_3 and phenol-*2,3,4,5,6*-d_5 TPD spectra. We plotted the total amount of H desorption and the total amount of D desorption from phenol-*2,4,6*-d_3 as a function of temperature. The total amounts are calculated as follows:

$$H = 2(\text{signal of 2 amu}) + (\text{signal of 3 amu})$$

$$D = 2(\text{signal of 4 amu}) + (\text{signal of 3 amu})$$

To correct for background H and H from OH, the 2 and 3 amu signals from C_6D_5OH were subtracted. The result is, as shown in Figure 8

$$\text{H at 450 K:H at 600 K:D at 450 K:D at 620 K} = 1:1:1:2$$

From this result, it is evident that, accounting for the two H and three D atoms in phenoxy-*2,4,6*-d_3, one H and one D desorb at 450 K. Therefore, we exclude paths 1 and 2, which will give either two D or two H desorption at 450 K, respectively.

HREELS data is in accord with TPD. We took HREELS of phenol-*2,4,6*-d_3/Pt(111) as a function of flashing temperature (Figure 9). After heating to 250 K, the ratio of the C−D and C−H stretching intensities was 3:2 as expected for labeled phenoxy, assuming the same excitation cross section for C−D and C−H modes. This result also holds at 350 K. As we flash the sample to 500 K (after 450 K hydrogen desorption), the C−D to C−H peak area ratio changes to 2:1 and is maintained at 600 K. These changes are consistent with TPD, confirming that the average stoichiometries are $C_6H_2D_3$ at the lower temperatures and C_6HD_2 at the higher temperatures. Finally, upon heating to 820 K, all the C−D and C−H signals disappear. The peak at 2070 cm^{-1} above 600 K is due to CO adsorption on the empty sites formed by hydrogen or benzene desorption.

Figure 10 shows HREELS of 2 ML phenol (A) and 1 ML phenol-d_5 (B) as a function of flashing temperature. At 125 K,

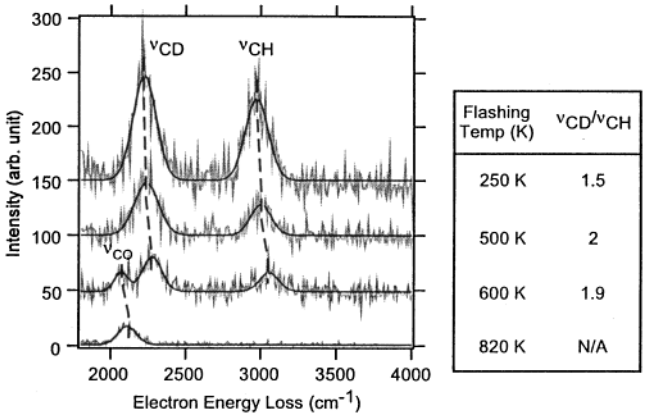

Figure 9. HREELS annealing set showing CD and CH stretching modes derived from phenol-*2,4,6*-d_3 on Pt(111). The data were taken at 125 K after flashing to the indicated temperature. The primary beam energy was 3 eV. The intensity changes indicate selective dehydrogenation. Raw data (gray lines) are fit (black lines) to remove noise contribution.

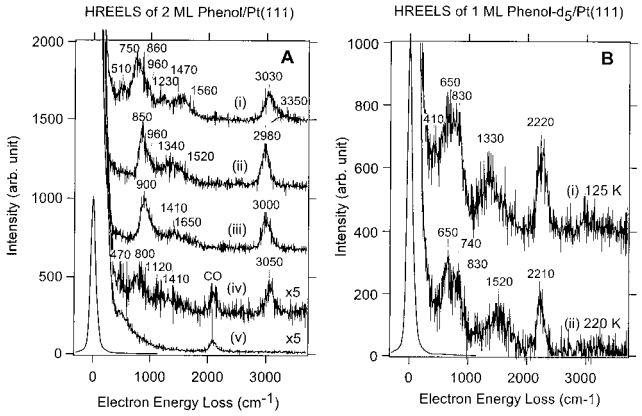

Figure 10. HREELS annealing set of (A) 2 ML phenol and (B) 1 ML phenol-d_5 on Pt(111) heated to (i) 125 K, (ii) 250/220 K, (iii) 350 K, (iv) 600 K, and (v) 820 K and recooled to take spectra. These data are taken with 3 eV primary beam energy.

2 ML phenol shows vibrational modes close to reported values, Figure 10 (A.i).[29,30] The detailed assignments are in Table 1. Generally, the OH stretching signal shifts from a sharp peak at 3655 cm^{-1} for vapor to a broad peak between 3130 and 3540 cm^{-1} for solution[29] owing to hydrogen bonding, and it shifts even further down to 1400−3000 cm^{-1} in organometallic complexes.[31] The OH stretching mode, clearly evident at 3300 cm^{-1} for 0.5 ML (Figure 6), is barely evident in Figure 10 (broad and weak, gray area) consistent with phenol adsorbed nearly parallel to the surface and joined to neighbors by intermolecular hydrogen bonds.

Upon heating to 250 K (A.ii), O−H bond dissociation occurs and changes the spectrum. The intense out-of-plane CH bending mode at 750 cm^{-1} and CH stretching mode at 3030 cm^{-1} shift to 850 and 2980 cm^{-1}, respectively. Also, a new peak at 1340 cm^{-1} appears and a peak at 1520 cm^{-1} becomes stronger while the peaks at 510 and 1230 cm^{-1} disappear. The spectrum of 1 ML phenol-d_5 (B.i) also compares favorably with the literature. Compared with phenol-h_6 data (A.i), there are larger shifts, as expected, of C−H(D) vibrational modes than of C−C or C−O vibrational modes. After flashing to 220 K (B.ii), the most prominent change is the peak shift from 1330 to 1520 cm^{-1}. Other peaks do not shift as much as in phenol-h_6, but relative intensities change. The 1520 cm^{-1} peak can be explained when compared with the phenol spectrum at 250 K (A.ii). Both spectra have signals at 1520 cm^{-1} that become stronger after flashing. This common feature is related to CC and/or CO vibrational modes and is due to structural changes accompanying O−H bond dissociation (see below).

Figure 10 (A.iii) shows that after flashing to 350 K, the overall features of the spectrum do not change significantly from the 250 K spectrum. The only difference is a blue shifting of the peaks. After flashing to 600 K, Figure 10 (A.iv), spectral features change and the peaks are at 470, 800, 1120, 1410, and 3050 cm^{-1}. The peak at 2070 cm^{-1} is due to CO adsorption from the background during data acquisition. This spectrum resembles literature spectra after *n*-but-1-ene or benzene are annealed at 600 K.[34,35] After annealing to 820 K, Figure 10 (A.v), the HREEL spectrum shows only adsorption of CO although there is a significant amount of other C as observed in XPS.

Discussion

Dissociation. On the basis of TPD, XPS, and HREELS results, the following reaction path is proposed

$$C_6H_5OH(g) \rightarrow C_6H_5OH(a) \quad \text{at 125 K} \qquad \text{(reaction 1)}$$

$$C_6H_5OH(a) \rightarrow C_6H_5O(a) + H(a) \quad \text{at 200 K} \qquad \text{(reaction 2)}$$

$$C_6H_5O(a) \rightarrow CO(g) + H_2(g) + \langle C_5H_3(a)\rangle \quad \text{at 490 K} \qquad \text{(reaction 3a)}$$

$$C_6H_5O(a) + H(a) \rightarrow C_6H_6(g) + O(a) \quad \text{above 400 K} \qquad \text{(reaction 3b)}$$

$$\langle C_5H_3(a)\rangle \rightarrow 3/2\ H_2(g) + 5C(a) \quad \text{above 550 K} \qquad \text{(reaction 4)}$$

where $\langle C_5H_3(a)\rangle$ indicates average stoichiometry, not necessarily an adsorbed species.We will discuss each step below.

Step 1. Adsorption and Geometry on the Surface. Hydrogen bonds dominate adsorbed phenol at 125 K. Many studies on phenol complexes in organometallics have reported η^6-binding with the phenol plane parallel to the center metal.[31,36−41] In a 3 ML HREELS experiment (not shown), the out-of-plane CH bending signal at 760 cm^{-1} was 2× the in-plane CH bending signals at 1230 and 1510 cm^{-1}. At and below 2 ML this ratio is larger indicating that parallel adsorption does not dominate for coverages greater than 2 ML. A suitable structural model is as follows. For coverages of less than 2 ML, adsorption places the C_6 plane closely parallel to the surface. For coverages of 2 ML or more, nonparallel orientations become important.

Step 2. Dissociation of Phenol and Adsorption Geometry of Phenoxy on the Surface. Unlike lower molecular weight alcohols where molecular desorption dominates, monolayer phenol completely dissociates by O−H bond scission upon heating to 200 K. Assuming the activation energy for O−H dissociation on Pt(111) is invariant among the alcohols, two factors are important. First, the activation energy for desorption of weakly adsorbed molecular species increases with molecular weight.[25,26] For small molecules, e.g., CH_3OH, the activation energy for desorption is less than that for dissociation so the former dominates. The desorption activation energy is higher for phenol owing to both π-bonding and increased molecular weight. π-character might even lower the activation energy of O−H bond dissociation. In this situation, dissociation dominates desorption of monolayer phenol.

There are several possible adsorption states of phenoxy prior to its dissociation. Assuming behavior similar to that in organometallic compounds, three models can be suggested:

TABLE 1: Vibrational Mode Assignments

mode	phenol[a]	C_6D_5OH[a]	η^5-C_6H_5O[b]	2 ML phenol/ Pt(111) at 125 K	2 ML phenol/ Pt(111) at 250 K	1 ML phenol-d_5/ Pt(111) at 125 K	1 ML phenol-d_5/ Pt(111) at 220 K
νOH(D)	3655(104)	3656		3300(broad)		3300(broad)	
νCH(D)	3052(4), 3046(12)	2262, 2258		3030	2980	2220	2210
νCC	1609(36), 1604(63)	1579, 1567		1560			
βCH(D) + νCC	1501(69), 1472(43)			1470−1500	1340		
νCC + βCH(D)	1344(18)	1404, 1372				1330(broad)	
βCC + νCC		1301					
νCO + νCC + βCH(D) + βCC	1261(51)	1179	1532−1635	1230	1520		1520
βOH(D) + νCC + βCH(D)	1197(106)	1204					
βCH(D) + νCC	1176(10), 1150(14)	869, 837, 831, 813				830	830
νCC + βCH(D)	1070(12)	1021					
γCH(D)	881(9)	776, 636, 624		860	960	650(broad)	740
νCC + βCC + νCO + βCH(D)	810(18)	754					
γCH(D) + γCO	752(75)	756		750	850		650
γCC	687(43)	513					
γCC + γCO + γCH(D)	503(20)	430		510		410	
βCO	410(8)	386					

[a] Vapor, frequency, and (intensity).[29,30] [b] In organometallic complex.[31−33]

SCHEME 2: For Phenoxy on Pt(111), Three Possible Adsorption Geometries. Darker Balls Represent C Atoms, and Lighter Balls Represent O Atoms

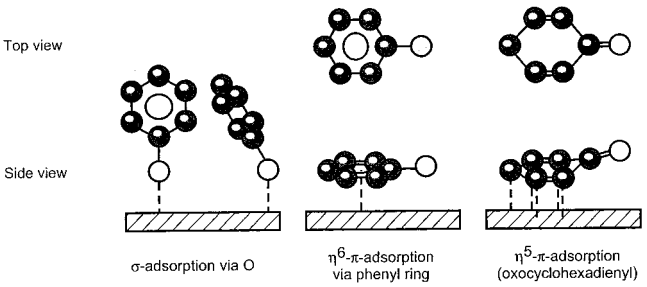

σ-adsorption via O (Ti),[32] η^6-π-adsorption (Ru),[42] η^5-π-adsorption (Rh, Ir, Ru, and Cr)[31−33,42,43] (See Scheme 2). If phenoxy bonds via O, the CO vibrational mode will be near 1250 cm^{-1}.[42] Also, if phenoxy bonds only through O to Pt, then as the O−H bond breaks, the phenyl ring plane will move from parallel toward perpendicular to the surface and the ratio of the out-of-plane to the in-plane C−H bending modes should be the reverse of the ratio before the O−H bond breaks. In the case of η^6-geometry, the CO vibrational mode will be near 1200 cm^{-1} (single bond) with a low cross section for HREELS owing to the parallel surface geometry of the C−O bond. X-ray crystallographic studies of organometallic analogues establish an η^5-geometry[32,33] with the CO bond tilted from the C2−C6 plane by at most 15°. In this structure the phenoxy species has an oxocyclohexadienyl geometry with the C(1) atom out of the plane (Scheme 2). For an η^5-geometry, IR studies report CO vibrational modes between 1520 and 1635 cm^{-1} characteristic of a double bond.[31−33,43] As we pointed out in the results section, after flashing to >220 K, a distinctive peak at 1520 cm^{-1} appears in both the phenol-h_6 and the phenol-d_5 spectra (Figure 10 (A.ii) and (B.ii)) and there is no significant change in the ratio of the out-of-plane to the in-plane C−H bending modes.

It is also noteworthy that, after annealing to 180 K, the O1s XPS (Figure 5B) shows additional intensity at lower binding energy. This indicates that electron density shifts to O atoms in the phenoxy species. This red shift is opposite from the blue shift in methoxy formation and also suggests that the phenoxy is not strongly bound to the surface via the O atom. A geometry that explains these observations is the η^5-π-adsorbed-quinoidal geometry. In this geometry, the bond lengths of C2−C3, C5−C6, and C1−O become shorter and the bond lengths of C1−C2, C3−C4, C4−C5, and C6−C1 become extended with respect to bonds in phenol. An ab initio calculation on an isolated phenoxy radical predicts a quinoidal structure.[44] While there is no detailed previous vibrational spectroscopic study with which to compare, this geometry agrees well with NEXAFS work indicating near parallel geometry and with the unique reactivity of phenol on Pt(111) (see below). Except for Mo(110) and Ag(110), earlier works suggest an adsorption geometry with the ring nearly parallel to the surface with O closer to the surface.

After annealing to 350 K (Figure 10A.iii) the C−H out-of-plane bending mode and C−H stretching mode shift to higher energies. Also, the peak at 1520 cm^{-1} shifts to 1650 cm^{-1} (C═C double bond). The C1s XPS peaks shift to lower binding energies by 0.3 eV after annealing to 400 K (Figure 5). Compared to the structure formed at 250 K, these observations are consistent with a form of oxocyclohexadienyl that has fully established C═C bond character.

Step 3. Dissociation of Phenoxy Species. Benzene desorption peaks, present only above 0.7 ML, shift to lower temperature as the initial coverage increases while the reverse holds for CO and D_2 peaks. This implies a competition between C−O dissociation and C−D formation to form benzene-d_6 and C−D and C−C dissociation to form D_2 and CO. At low coverages, many unoccupied sites are available throughout the TPD, so C−C and C−D bond dissociation dominate and no C_6D_6 forms, whereas for higher coverages, C−C and C−D bond cleavages are inhibited by crowded surroundings so C−D bond formation to form C_6D_6 becomes competitive below 470 K. Consistent with these notions, there is no benzene dissociation when it is dosed onto Pt covered by 0.25 ML of Bi.[20] We conclude that, above a critical initial phenol coverage, benzene desorption dominates until the local coverage drops enough to favor the C−D bond breaking. The 500 K shoulder in benzene desorption (Figure 3C) is attributed to temporary local coverage increase that promotes benzene formation.

In the results section, we reported stepwise preferential dehydrogenation at 490 K accompanied with CO desorption at the same temperature. There are two emerging questions regarding this dissociation step. First, is the dissociation concerted or successive? If it is not concerted, do the C−C or the C−H bonds break first? Second, do the hydrogen atoms dissociate from ortho- and meta-positions or meta- and para-

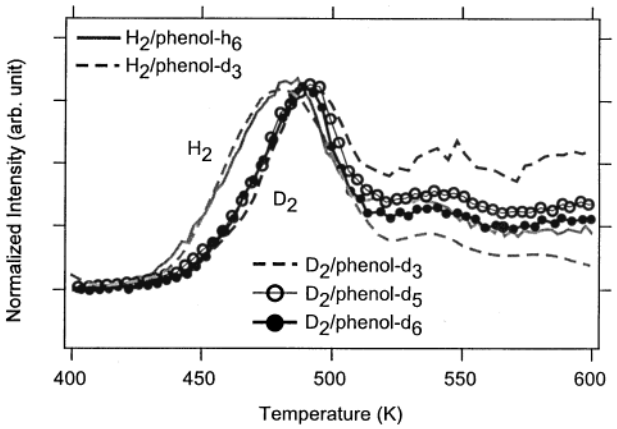

Figure 11. 490 K H_2 (gray lines) and D_2 (black lines) desorption peak from various isotopic phenols. The H_2 desorption begins 10 K lower and peaks 5 K lower than the D_2 desorption, reflecting a lower activation energy for breaking C−H. The constant leading edges and peak positions of the H_2 and D_2 desorptions, regardless of source, indicate that the position of H and D in the C_6 ring do not alter the activation energies for breaking carbon−hydrogen bonds.

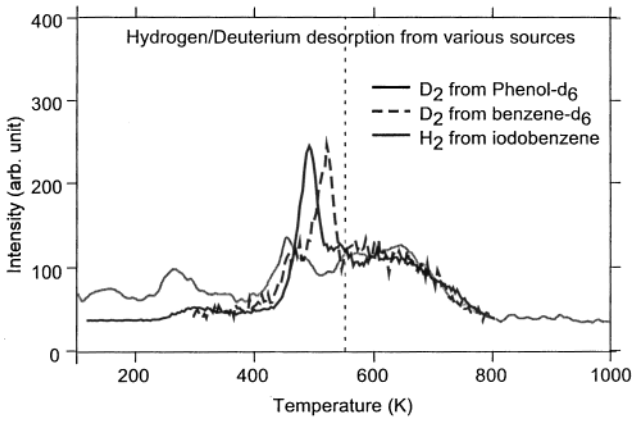

Figure 12. Hydrogen and deuterium desorption from 1 ML of phenol-d_6 (black solid line), benzene-d_6 (black dashed line), and iodobenzene (gray solid line). The desorption spectra are normalized with respect to the peak at 620 K. The common features above 550 K imply that a common distribution of intermediate species is produced from all three chemicals.

positions? The answer to those questions lies in the following observations.

Since directly dosed CO and H_2/D_2 desorb at much lower temperatures, the 490 K peaks of CO and D_2 are reaction-limited. A rough estimate of the activation energy for this process is 128 kJ/mol (31 kcal/mol). Figure 11 shows normalized H_2 and D_2 desorption peaks between 400 and 600 K from various isotopic phenols. Two things are important. First, the H_2 desorption begins 10 K lower and peaks 5 K lower than the D_2 desorption, reflecting an isotopic effect in the activation energy for C−H bond breaking. Second, the H_2 desorption peaks are the same regardless of whether H or D atoms occupy the ortho- and para-positions. Similarly, the D_2 desorption peaks are the same regardless of H or D in meta-positions. Therefore, the C−H/C−D bond activation is the rate-limiting step for H_2/D_2 desorption with the activation energy independent of position in the C_6 ring. On the basis of the same argument, C−H bond dissociation is the rate-limiting step in phenoxy decomposition on Ni(110) and Al(111).[7,11,12] In these reports, when phenol was labeled with H in the meta-positions and D in the others, the H_2 peak shifted to higher temperatures indicating that the first C−H bond dissociation in the phenoxy was selectively in ortho- or para-positions.

The difference can be explained by the adsorption geometry. As discussed earlier, phenoxy on Pt(111) is bound in an η^5-π-geometry via the C2, C3, C4, C5, and C6 atoms. This form differs from free phenoxy in solution or phenoxy bonded via O, where ortho- and para-positions withdraw electron density either from O or from metal bonded to O, so that reactions at the ortho- and para-positions are favored. When phenoxy rearranges to oxocyclohexadienyl, the ortho-, para- and meta-positions become equivalent.

The following model is proposed. After gaining enough thermal energy, C−H/C−D bonds in one meta- and one ortho- or para-position break. The energy released in this process is enough to cause dissociation of already weak C1−C2 and C1−C6 bonds, a process leading to CO. Since there are two remaining weak C−C bonds in the resulting C_5 species, further C−C dissociation is plausible.

Step 4. Dissociation of Species with C_5H_3 Stoichiometry: Comparison with Benzene and Iodobenzene. In Figure 8, the calculated high-temperature H desorption peaks at 600 K while D peaks at 620 K. There are two factors to consider: (1) the activation energy difference between C−H and C−D bonds and (2) the difference in the position on the ring. Figure 12 shows H_2/D_2 desorption spectra from 1 ML of phenol-d_6, benzene-d_6, and iodobenzene. As discussed above, phenol-d_6 shows 1:2:3 deuterium desorption ratio at 300, 490, and 620 K, respectively. Iodobenzene gives 1:1:3 ratio at 280, 470, and 620 K, respectively.[35] Benzene-d_6 gives 1:2:3 ratio at 490, 530, and 620 K, respectively. Although the peak positions vary slightly, the general desorption features, ratios, and particularly the broad peak at 620 K remain the same. This similarity strongly suggests the presence of the same intermediate species at 550 K for all three molecules and a similar dissociation process above 550 K.

The HREEL spectrum of phenol after annealing at 600 K shows peaks at 470, 800, 1120, 1410, and 3050 cm^{-1} (Figure 10A.iv). Iodobenzene on Pt(111) shows peaks at 770, 3020 cm^{-1} with a small hint at 1400 cm^{-1} after annealing at 600 K.[35] The HREELS work of benzene on Rh(111) after annealing at 470 K[46] has reported peaks at 475, 800, 1365, and 3008 cm^{-1}, and C_2H was suggested to be the intermediate at that temperature, on the basis of the comparisons with organometallic study data and other C_2 hydrocarbon studies on Pd, Ni, and Pt.[45] For example, ethylene on Pt(111) shows peaks at 420, 800, 1170, 1430, and 3000 cm^{-1}.[45] Although C_2H is plausible, there is another attractive candidate, C_3H_3 (propargyl). Organometallic η^3-propargyl complexes are well-known.[47,48] For example, $[(PPh_3)_2Pt(\eta^3\text{-}CH_3\mathbf{C}H\mathbf{C}\equiv\mathbf{C}\text{-}t\text{-}C_4H_9)]^+$ shows peaks at 636, 699, 745, 835, 844, 919, 999, 1030, 1097, 1146, 1365, 1437, 1481, 2905, 2929, 2950, 2970, and 3056 cm^{-1}, and $[(PPh_3)_2Pt(\eta^3\text{-}CH_3\mathbf{C}H\mathbf{C}\equiv\mathbf{C}CH_3)]^+$ shows peaks at 636, 694, 753, 999, 1031, 1096, 1436, 1481, 2921, 3007, 3056, and 3073 cm^{-1}.[48] The bands near 700, 1100, 1400, and 3050 cm^{-1} are consistent with HREELS data for the decomposition of adsorbed C_6 cyclic hydrocarbons above 550 K. Such C_3H_3 species are also stable and can dimerize to benzene on Pd(111).[49]

At this point, it has proven impossible to determine by HREELS whether the C_5H_3 average stoichiometry is $2C_2H$ + CH, C_3H_3 + C_2, or a mixture of these. However, we exclude $2C_2H$ + CH through the following discussion that focuses on the measured isotopic dihydrogen that desorbs. The H/D isotope ratio is unity for the 490 K desorption peak from phenol-*2,4,6*-d_3, Figure 8. To realize this ratio, there are only two possible bond dissociation channels. If ortho-CH and meta-CD bonds break in phenol-*2,4,6*-d_3, the resulting transient species will be

SCHEME 3: Model Describing Thermal Reaction Paths of Phenol-*2,4,6-d*$_3$ on Pt(111)

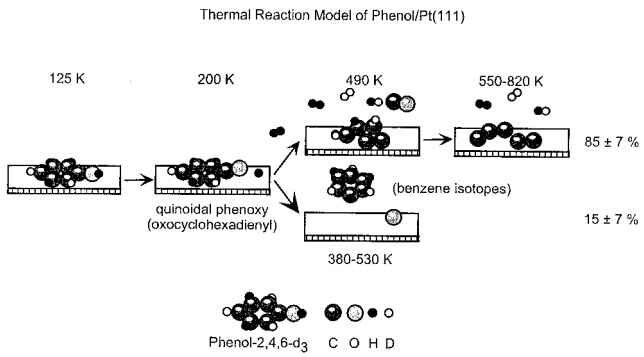

−C(2)═C(3)−C(4)D−C(5)H═C(6)D−. C_2 and C_3HD_2 will form by breaking only one bond, C(3)−C(4), whereas to form $2C_2H$ + CH (isotopically labeled) involves breaking a double bond and a single bond. On the other hand, if meta- and para-bonds break, the resulting transient species will be −C(2)D═C(3)−C(4)−C(5)H═C(6)D−. The path from this intermediate to either set of products requires breaking at least two bonds. On the basis of simplicity constrained by the observed H/D ratio in the 490 K dihydrogen TPD peak, we favor ortho- and meta-position C−H/C−D dissociation and C_2 and C_3H_3 formation as the most likely initial step for phenoxy dissociation.

Thermal Reaction Model. In this section, we have divided the thermal reaction process of phenol on Pt(111) into four steps and discussed the most plausible reaction pathways and adsorption geometries of major intermediates. Scheme 3 shows the schematic diagram of each step. This model is for initial coverages higher than 1 ML. For simplicity, we omitted the second layer and the multilayer in the figure. There are two major phenoxy reaction pathways. The first is C−H/C−D and C−C bond dissociation producing gas-phase CO and dihydrogen (reaction 3a). One ortho- and one meta-position C−H/C−D dissociate selectively. After C−H/C−D and C−C bond dissociation, C_2(a) and C_3H_3(a) remain on the surface. The intermediate adsorbed species decompose upon heating. The second pathway involves C−O bond dissociation (reaction 3b) and is very similar to that of benzene-like molecules. The resulting phenyl recombines with H and forms benzene. A major factor in determining the ratio of the two pathways is surface crowdedness. Below 0.5 ML coverages, full decomposition is favorable. Above 1 ML, the surface is very crowded and the reaction probabilities are 85 ± 7% and 15 ± 7%, respectively. These values are based on XPS and TPD of hydrogen isotopes, benzene isotopes, and CO. Between 0.5 and 1 ML coverages, the ratio of products lies between those of 0.5 and 1 ML. During annealing to 1100 K, the intermediate species on the surface further decompose producing homogeneous carbide as shown in XPS.

Conclusions

Using various deuterium-labeled forms, we studied the thermal reaction chemistry of phenol on Pt(111) with TPD, HREELS, and XPS. Phenol adsorbs molecularly at 125 K, with the ring plane parallel to the surface. During heating, O−H bond scission is complete by 200 K. Compared to systems involving either alkoxides or phenyl groups, the phenoxy system is unique. The O in phenoxy mediates redistribution of electron density and induces a unique adsorption geometry, quinoidal-η^5-π-adsorption via the C2 through C6 atoms with the C1 atom tilted away from the ring plane. The phenoxy rearranges to oxocyclohexadienyl upon heating. Above 0.7 ML phenol coverage, oxocyclohexadienyl follows two different pathways. (1) 85 ± 7% forms CO(g), H_2(g), C_2(a), and C_3H_3(a) at 490 K; the latter dehydrogenates to H_2(g) and C(a) above 550 K. In this mechanism, the evidence favors initiation by breaking one ortho- and one meta-C−H bond. (2) About 15 ± 7% reacts like a monosubstituted benzene and forms benzene(g) and O(a) between 380 and 530 K. Below 0.5 ML coverage, no CH-containing species desorb because, at such low coverages, C−C and C−H bond activation occurs more readily than the C−O bond activation. When the local coverage is high, C−H and C−C bond breaking are inhibited because catalytic sites are blocked. Thus, C−O bond cleavage and C−H bond formation become competitive. For adsorbed phenol, iodobenzene, and benzene, there are common vibrational spectra and desorption features above 550 K, strongly suggesting a common intermediate species. We present evidence favoring propargyl, C_3H_3. Carbidic carbon remains after 1100 K annealing.

Acknowledgment. This work was supported by the U.S. Department of Energy, Office of Basic Energy Sciences, and by the Robert A. Welch Foundation.

References and Notes

(1) Zhuang, S. X. *Chinese Chemical Lett.* **1996**, *7*, 661.
(2) Lu, L.; Salaita, G. N.; Laguren-Davidson, L.; Stern, D. A.; Wellner, E.; Frank, D. G.; Batina, N.; Zapien, D. C.; Walton, N.; Hubbard, A. T. *Langmuir* **1988**, *4*, 637.
(3) Xu, X.; Friend, C. M. *J. Phys. Chem.* **1989**, *93*, 8072.
(4) Bu, H.; Bertrand, P.; Rabalais, J. W. *J. Chem. Phys.* **1993**, *98*, 5855.
(5) Guo, X.-C.; Madix, R. J. *Surf. Sci.* **1995**, *341*, L1065.
(6) Steinmüller, D.; Ramsey, M. G.; Netzer, F. P. *Surf. Sci.* **1992**, *271*, 567.
(7) Russell, J. N.; Sarvis, S. S.; Morris, R. E. *Surf. Sci.* **1995**, *338*, 189.
(8) Serafin, J. G.; Friend, C. M. *Surf. Sci.* **1989**, *209*, L163.
(9) Liu, A. C.; Friend, C. M. *Surf. Sci. Lett.* **1990**, *236*, L349.
(10) Ramsey, M. G.; Rosina, G.; Steinmüller, D.; Graen, H. H.; Netzer, F. P. *Surf. Sci.* **1990**, *232*, 266.
(11) Russell, J. N.; Leming, A.; Morris, R. E. *Surf. Sci.* **1998**, *399*, 239.
(12) Bartlett, B.; Valdisera, J. M.; Russell, J. N. *Surf. Sci.* **1999**, *442*, 265.
(13) Myers, A. K.; Benziger, J. B. *Langmuir* **1989**, *5*, 1270.
(14) Richardson, N. V.; Hofmann, P. *Vacuum* **1983**, *33*, 793.
(15) Solomon, J. L.; Madix, R. J.; Stohr, J. *Surf. Sci.* **1991**, *255*, 12.
(16) Carbone, M.; Piancastelli, M. N.; Casaletto, M. P.; Zanoni, R.; Besnard-Ramage, M. J.; Comtet, G.; Dujardin, G.; Hellner, L. *Surf. Sci.* **1999**, *419*, 114.
(17) Zhu, X. Y.; Wolf, M.; White, J. M. *J. Chem. Phys.* **1992**, *97*, 605.
(18) Chastain, J. *Handbook of X-ray Photoelectron Spectroscopy: A Reference Book Standard Spectra for Identification and Interpretation of XPS Data*; Perkin-Elmer, Physical Electronics Division: Eden Prairie, MN, 1992.
(19) Norton, P. R.; Davies, J. A.; Jackman, T. E. *Surf. Sci.* **1982**, *122*, L593.
(20) Campbell, J. M.; Seimanides, S.; Campbell, C. T. *J. Phys. Chem.* **1989**, *93*, 815.
(21) Chittenden, C. N.; Pylant, E. D.; Schwaner, A. L.; White, J. M. *Handbook of Surface Imaging and Visualization*; Hubbard, A. T., Ed.; CRC Press: New York, 1995; pp 817−45.
(22) Lide, D. R. Ed. *CRC Handbook of Chemistry and Physics*, 76th ed.; CRC Press: Boca Raton, FL, 1995; pp 6−122.
(23) Fisher, G. B.; Gland, J. L. *Surf. Sci.* **1980**, *94*, 446.
(24) Christmann, K.; Ertl, G.; Pignet, T. *Surf. Sci.* **1976**, *54*, 365.
(25) Sexton, B. A.; Rendulic, K. D.; Hughes, A. E. *Surf. Sci.* **1982**, *121*, 181.
(26) Vannice, M. A.; Erley, W.; Ibach, H. *Surf. Sci.* **1991**, *254*, 12.
(27) Ohta, T.; Fujikawa, T.; Kuroda, *J. Bull. Chem. Soc. Jpn.* **1975**, *48*, 2017.
(28) Chastain, J., King, R. C., Jr., Eds. *Handbook of X-ray Photoelectron Spectroscopy*; Physical Electronics: Eden Prairie, MN, 1995.
(29) Keresztury, G.; Billes, F.; Kubinyi, M.; Sundius, T. *J. Phys. Chem. A* **1998**, *102*, 1371.
(30) Bist, H. D.; Brand, J. C. D.; Williams, D. R. *J. Mol. Spectrosc.* **1967**, *24*, 413.

(31) White, C.; Thompson, S. J.; Maitlis, P. M. *J. Organomet. Chem.* **1977**, *127*, 415.
(32) Cetinkaya, B.; Hitchcock, P. B.; Lappert, M. F.; Torroni, S.; Atwood, J. L.; Hunter, W. E.; Zaworotko, M. J. *J. Organomet. Chem.* **1980**, *188*, C31.
(33) Dahlenburg, L.; Höck, N. *J. Organomet. Chem.* **1985**, *284*, 129.
(34) Avery, N. R.; Sheppard, N. *Proc. R. Soc. London, Ser. A* **1986**, *405*, 1.
(35) Cabibil, H.; Ihm, H.; White, J. M. *Surf. Sci.* **2000**, *447*, 91.
(36) Fischer, E. O.; Öfele, K.; Essler, H.; Fröhlich, W.; Mortensen, J. P.; Semmlinger, W. *Chem. Ber.* **1958**, *91*, 2763.
(37) Natta, G.; Calderazzo, F.; Santambrogio, E.; *Chim. Ind. Milan* **1958**, *40*, 2763.
(38) Fritz, H. P.; Kreiter, C. G. *J. Organomet. Chem.* **1967**, *7*, 427.
(39) Besançon J.; Tirouflet, *J. Rev. Chim. Min.* **1968**, *5*, 363.
(40) Green, M.; Kuc, T. A. *J. Chem. Soc., Dalton Trans.* **1972**, 832.
(41) Wu, A.; Biehl, E. R.; Reeves, P. C. *J. Chem. Soc., Perkin Trans. 2* **1972**, 449.
(42) Cole-Hamilton, D. J.; Young, R. J.; Wilkinson, G. *J. Chem. Soc., Dalton Trans.* **1976**, 1995.
(43) Trahanovsky W. S.; Hall, R. A. *J. Am. Chem. Soc.* **1977**, *99*, 4850.
(44) Re, S.; Osamura, Y. *J. Phys. Chem.* A **1998**, *102*, 3799.
(45) Baró, A. M.; Ibach, H. *J. Chem. Phys.* **1981**, *74*, 4194.
(46) Koel, B. E.; Crowell, J. E.; Bent, B. E.; Mate, C. M.; Somorjai, G. A. *J. Phys. Chem.* **1986**, *90*, 2949.
(47) (a) Gotzig, J.; Otto, H.; Werner, H. *J. Organomet. Chem.* **1985**, *287*, 247. (b) Jia, G.; Rheingold, A. L.; Meek, D. W. *Organometallics* **1989**, *8*, 1378. (c) Bianchini, C.; Peruzzini, M.; Zanobini, F.; Frediani, P.; Albinati, A. *J. Am. Chem. Soc.* **1991**, *113*, 5453. (d) McMullen, A. K.; Selegue, J. P.; Wang, J.-G. *Organometallics* **1991**, *10*, 3421. (e) Casey, C. P.; Yi, C. S. *J. Am. Chem. Soc.* **1992**, *114*, 6597. (f) Blosser, P. W.; Gallucci, J. C.; Wojcicki, A. *J. Am. Chem. Soc.* **1993**, *115*, 2994. (g) Stang, P. J.; Crittel, C. M.; Arif, A. M. *Organometallics* **1993**, *12*, 4799. (h) Huang, T.-M.; Chen, J.-T.; Lee, G.-H.; Wang, Y. *J. Am. Chem. Soc.* **1993**, *115*, 1170.
(48) Stang, P. J.; Crittell, C. M.; Arif, A. M. *Organometallics* **1993**, *12*, 4799.
(49) Caldwell, T. E.; Abdelrehim, I. M.; Land, D. P. *J. Am. Chem. Soc.* **1996**, *118*, 907.